JOURNAL OF QUATERNARY SCIENCE (2025) **40**(5) 862–875 ISSN 0267-8179. DOI: 10.1002/jqs.3719

JQS Journal of Quaternary Science QRA Quaternary Research Association

Dating the Middle Palaeolithic of Fumane Cave by the combined ESR/U-series method

CHRISTOPHE FALGUÈRES,[1] GIULIA GRUPPIONI,[1,2] JEAN JACQUES BAHAIN,[1] JEAN MICHEL DOLO[1] and MARCO PERESANI[2,3]*

[1]HNHP (Histoire Naturelle des Humanités Préhistoriques) UMR7194 MNHN-CNRS-UPVD, Institut de Paléontologie Humaine, Paris, France
[2]Department of Humanities, Prehistoric and Anthropological Sciences Unit, University of Ferrara, Ferrara, Italy
[3]National Research Council, Institute of Environmental Geology and Geoengineering, Milano, Italy

Received 25 December 2024; Revised 2 April 2025; Accepted 4 April 2025

ABSTRACT: Fumane Cave, located in Northern Italy, is a major prehistoric site for understanding late Neandertal and early modern human behaviours. The cave contains a 12-m-thick stratigraphic sequence of Middle and Upper Palaeolithic layers, which have yielded a number of flint artefacts and faunal remains. The upper part of the stratigraphic sequence is well-dated using radiocarbon analysis, placing the last Middle Palaeolithic occupations at ca. 44–45 ka cal BP and the first Upper Palaeolithic occupations (Uluzzian and Aurignacian) after around 43 ka cal BP. However, the lower part of the stratigraphic sequence remains less well-documented chronologically. Previous thermoluminescence (TL) dating placed the entire sequence within the last climatic cycle, following the last Interglacial stage (MIS 5e). In this study, we present a revised chronology for the Middle Palaeolithic levels at Fumane Cave, based on combined Electronic Spin Resonance/Uranium (ESR/U)-series dating of herbivorous teeth spanning much of the sequence. Our results diverge from earlier TL data, indicating that the oldest layers date to MIS 7–6 (units S9–S3) and MIS 6–5 (units BR12–BR9). For the late Mousterian (units A11–A4) and the Upper Palaeolithic (unit A2), recalculated ages using new *in situ* gamma measurements align with existing radiocarbon and TL dates. However, our findings highlight the methodological challenges of applying ESR/U-series dating to samples younger than 50 ka, particularly in heterogeneous layers. These new results suggest that Middle Palaeolithic occupations at Fumane Cave spanned over 200 ka, covering the two most recent climatic cycles. This extended temporal framework parallels that of San Bernardino cave, another key site in Northern Italy, and underscores the prolonged presence of Levallois technology in the region. © 2025 The Authors *Journal of Quaternary Science* Published by John Wiley & Sons Ltd.

KEYWORDS: cave; ESR/U-series dating; Italy; Middle Pleistocene; tooth

Introduction

The Fumane cave, located in the Monti Lessini Region of Northeastern Italy (Fig. 1(1),(2)), contains one of the most significant Middle and Upper Palaeolithic records in Europe. Excavations have been ongoing since 1998. The cave is part of an inactive Neogene karst complex, opening at the base of a carbonate sandstone cliff composed of alternating massive banks of oolithic calcarenites, characterised by typical cross-lamination, and micritic banks of metric thickness separated by discontinuities. In the stream valley where the cave opens, this formation, known as Ooliti di San Vigilio (Upper Lias), is extensively dolomitised. The karst complex includes a wide cavity, likely a natural pit, filled at its base with present-day explored deposits with residual dolomitic sands of unknown thickness. A remnant of the original pit wall remains visible today along the eastern sector of the current archaeological area's ground level. The pit walls and the sedimentary deposits preserved on them were partially eroded due to the morphological evolution of the stream valley and were eventually exposed by road construction activities in the mid-20th century. Currently, the site is accessed via a sheltered entrance, approximately 30 m² in size, located at the upper level of the karst complex. The current morphology of the cave is the result of substantial collapses—caused by repeated frost action—impacting the massive calcarenite banks, as well as the weathering of micritic layers. The cave measures approximately 11 m in width and 22 m in length, with the top surface of the deposit near the cave mouth lying about 3.8 m below the cave ceiling.

The purpose of this study is to establish a reliable chronology for the Middle Palaeolithic layers of Fumane Cave using the Electronic Spin Resonance/Uranium (ESR/U)-series method. The results will be compared with those obtained through thermoluminescence and assessed for consistency with the currently available radiocarbon chronology, which constrains the transition from the latest Mousterian occupations (units A5–A6) to the Upper Palaeolithic occurrences (units A3 and A2) (see Higham *et al.*, 2009; 2014; Douka *et al.*, 2014; Marín-Arroyo *et al.*, 2023).

Fumane sedimentary and cultural sequence

The karst complex at Fumane contains a 12-m-thick sedimentary sequence, measured from the present-day ground level at the road to the top above the cave entrance. This sequence is divided into four macro-units—S, BR, A and D—from bottom

*Correspondence: M. Peresani, as above.
E-mail: marco.peresani@unife.it

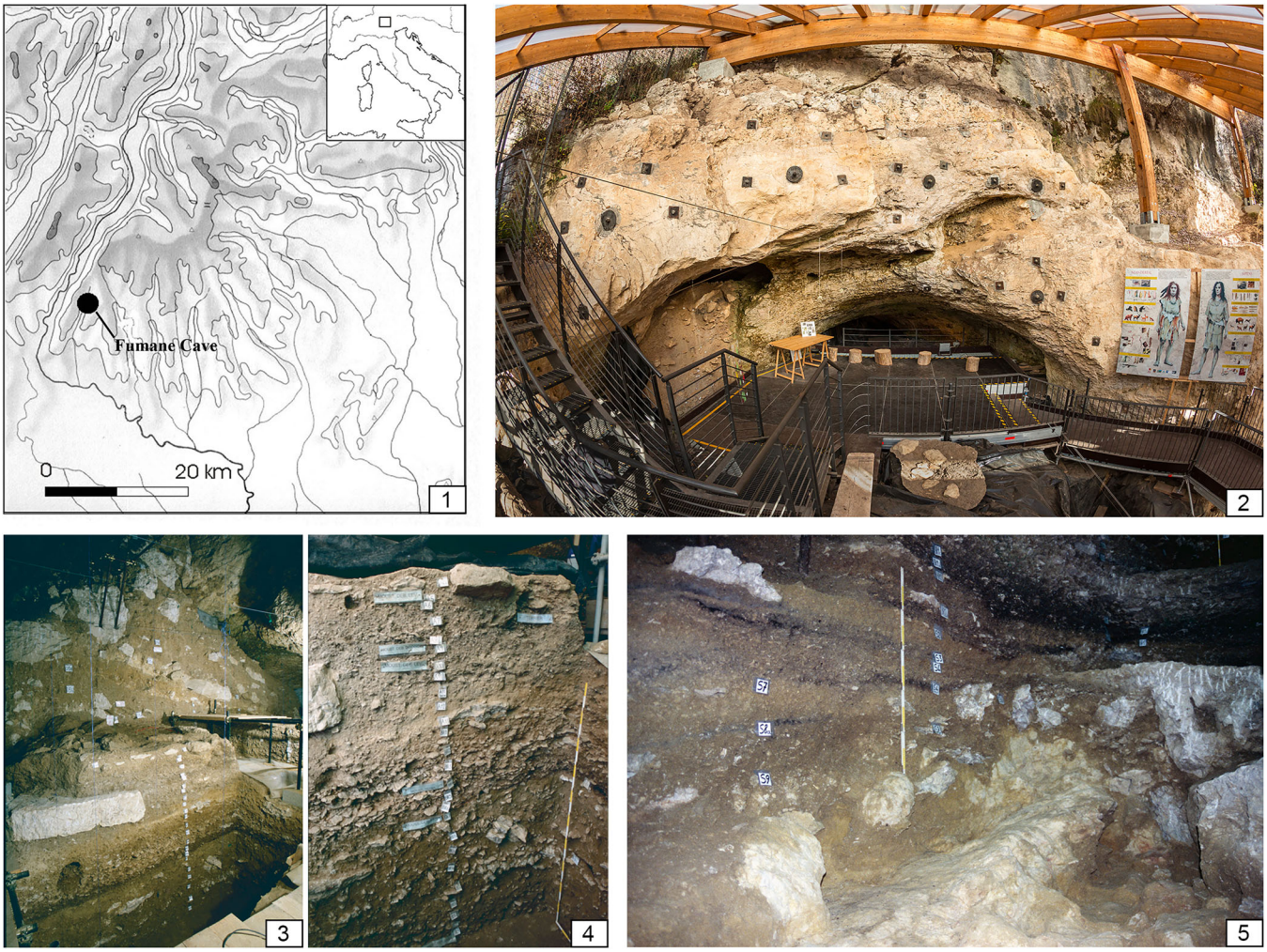

Figure 1. (1) Position of Fumane in the Monti Lessini Plateau; (2) the present-day entrance of the cave with the main tunnels, A on the left and B at the centre; (3) the stratigraphic sequence exposed on the main sagittal section running from the outside to the inner cave along tunnel B (macro-unit D and units A1 and A2 visible on the upper section were removed in 1995); (4) anthropic units A3 to A11 and part of macro-unit BR on the sagittal section still in place; (5) the macro-unit S with units from S9 to S2 exposed on the sagittal section. [Color figure can be viewed at wileyonlinelibrary.com]

to top, based on their lithological composition and archaeological content (see references in Peresani, 2022). These sediments are currently accessible from several sections: the main cut facing the road (residual-base sandy plug, macro-units S and BR); the three pit sections opened in 1992, 1993 and 1995 (lower boulders lying on the residual sandy plug and units from S10 to A3); the section at the entrance of tunnel A (from A9 to D1e); the sections in the cave-mouth (from A9 to D1e and A6 to D1e); the walls of the trench opened in 1989 and 1990 in the entrance of the cave (layers A12 to A10) and the small section preserved at the entrance of tunnel C (layers A10 to D6). Based on integrated geophysical investigations conducted in 2013, the volume of the largest sedimentary component, where remains are more likely to be found, was estimated at approximately 50–75 m in the uppermost 3 m of deposits (Abu Zeid *et al.*, 2019).

- The sedimentary sequence (Fig. 2) has been documented in the field and investigated through its macroscopic features, texture, heavy mineral content, micromorphology and magnetic properties, as preliminarily presented by Cremaschi *et al.* (2005) and with detail for macrounits A and D by Kehl *et al.* (2025). Above the weathered bedrock and the residual yellow, massive dolomite sandy plug, **macro-unit S** consists of sub-horizontal layers made of dolomite sand, angular stones, surface weathered boulders and traces of human occupation (Fig. 1(3)). These traces, showing varying grades of anthropisation, are scattered across layers S10 to S1, with a total thickness of 1.4 m. Pedogenesis affected the bedrock under conditions of climatic instability, followed by moderate roof degradation and hydrological redistribution of dolomite sands.
- The overlying **macro-unit BR** forms a massive sedimentary body made of stones and aeolian dust deposits (Fig. 1(4)). Layer BR11, with a thickness of 0.4 m, contains a dense accumulation of cultural material, including articulated ungulate bones, knapped chert artefacts, charcoal and associated combustion features. Units BR10 to BR7a form another massive sedimentary body, with a total thickness of 1.6 m. Unit BR6 represents an anthropogenic level lying on BR7, while units BR5 and BR4 consist of coarse open-work, frost-shattered breccia, sealing scattered fireplaces and associated cultural material (Peresani *et al.*, 2023). Units BR3 to BR1 are composed of stones and fine sediment.
- **Macro-unit A** includes several horizontal layers from A13 to A1, mostly composed of residual dolomite sands (layers A13-A12), angular fine to medium-sized stone layers (levels in A10 complex, layers A7, A4), stones, slabs and fine material (layer A3), as well as varying amounts of organic and cultural material (A11, levels in A10 and A9 complexes, A6, A2-A1) (Peresani, 2022; Kehl *et al.*, 2025) (Fig. 1(5)). The sand and aeolian silt content gradually increase from

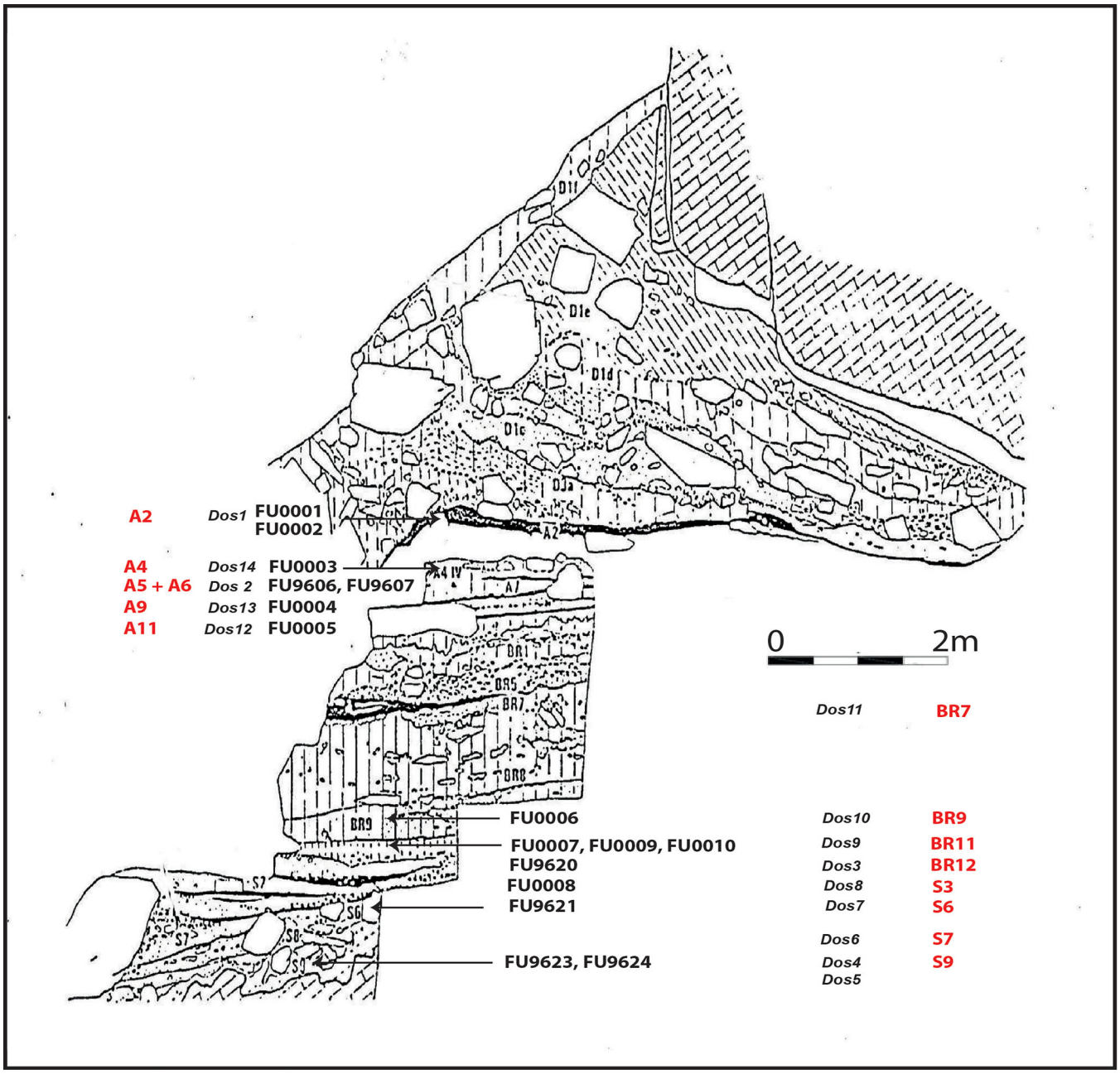

Figure 2. Stratigraphic sequence of Fumane site with location of the different teeth and the dosimeters used for the ESR/U-series dating (modified from Peresani *et al.*, 2008). [Color figure can be viewed at wileyonlinelibrary.com]

the sheltered area toward the exterior, becoming almost exclusive in the latter. These sediments are generally loose or densely packed but never intensively cemented.

– The cave entrance and main tunnels are sealed by **macro-unit D**, located at the top of the sequence. This unit is mostly composed of boulders resulting from rockfalls, along with stones, sand and varying amounts of aeolian dust. The thickness of the layers gradually diminishes towards the cave mouth, where post-depositional deformations occur under the influence of periglacial conditions at the onset and during MIS2 (Kehl *et al.*, 2025).

Palaeoenvironmental assessments of macro-units S and BR, which are the primary focus of our dating programme, have been conducted based on sedimentological and palaeontological analyses, albeit only at a preliminary level (Fiore *et al.*, 2004; Cremaschi *et al.*, 2005). The macromammal assemblages represent a rich and diverse fauna introduced into the cave and exploited by humans. In macro-unit S, cervids dominate over caprids; however, episodes of climate cooling identified in layers S9 and S3 are marked by a reversal of this trend, with caprids becoming more prevalent. In macro-unit BR, cervids remain dominant during the initial phases but there is a noticeable increase in caprids, particularly in BR6, peaking in BR1. In macro-unit A, cervids dominate in units A13-A12 but are abruptly replaced by ibex and chamois in Unit A2. This shift coincides with the first Aurignacian occupation and the spread of alpine grasslands (Fiore *et al.*, 2004).

Evidence of repeated human occupations is recorded throughout macro-unit S, while in macro-unit BR, aside from the dense accumulation of cultural remains in BR11, the evidence mostly consists of dispersed lithic artefacts, faunal remains and hearths associated with scattered tools and bones indicative of short-term occupations (i.e., in BR6, Cremaschi *et al.*, 2002). Within these assemblages, the Levallois method was the exclusive flaking technique used in all units from S9 to A4. Exceptions include BR6 to BR4, where Quina industries are documented (Peresani

et al., 2023) and in A9, where Discoid technology was the most frequently used. Most of the artefacts are remarkably well-preserved, exhibiting either primary or fractured fresh edges. While devoid of abrasions, their surfaces are often slightly patinated, obscuring the finer chromatic features and micropaleontological content of the chert.

Traces of more intense human occupations have been identified within macro-unit A. Mousterian living floors are present in A11, A10, A9, A6-A5, A4, Uluzzian in A3 and Protoaurignacian and Early Aurignacian in A2-A1 and D3 (D3d, D3b-D3a, D1c and correlated units) respectively (Falcucci *et al.*, 2020). Dispersed Gravettian artefacts were recovered in unit D1d (see Peresani, 2022 and references therein).

Current chronological context

A substantial set of radiocarbon dates demonstrate that the late Mousterian, Uluzzian, Aurignacian and Gravettian frequentations fall within MIS3, extending up to the onset of MIS2 (Higham *et al.*, 2009; Douka *et al.*, 2014; Marín-Arroyo *et al.*, 2023) as also confirmed by ESR/U-series and TL chronology for the late Mousterian (Martini *et al.*, 2001; Peresani *et al.*, 2008; Peresani, 2022 for summary). The chronological range of unit A9 is constrained by a minimum age of 47.6 ka cal BP (Peresani *et al.*, 2008; Higham *et al.*, 2014) and by the lower chronological boundary of layer A5 + A6 at 44.8 ka cal BP. This date also marks a minimum age for layers A6 and A7. To refine the chronological resolution from A6 down to A11, a new set of radiocarbon dates is required. The final Mousterian phase, spanning from A5 + A6 to A4, dates between 44.8 and 42.2 ka cal BP (Higham *et al.*, 2009) and is succeeded by the Uluzzian, followed by the Protoaurignacian in A2 and A1, dating to 41.2–40.4 ka cal BP (Higham *et al.*, 2009; Douka *et al.*, 2014; Marín-Arroyo *et al.*, 2023). Layers D3, D6 and D3 + D6 represent the late Protoaurignacian, dated to 38.9–37.7 ka cal BP (Higham *et al.*, 2009; Falcucci *et al.*, 2020) while unit D1d, associated with the Gravettian, has a maximum age of 35 ka cal BP (see discussion in Falcucci and Peresani, 2019).

The chronologies for macro-units BR and S, however, remain incomplete. Thermoluminescence analyses (Martini *et al.*, 2001) dated two samples from BR12-BR11 and S7 to 56 ka and 80 ka, respectively, suggesting that the entire sequence falls within the last glacial period. In contrast, a set of ESR/U-series combined dates provides ages approximately 100 ka older for the same units, placing the sequence within the two last climatic cycles (Gruppioni, 2004). To address this discrepancy and determine whether the stratigraphic sequence is confined to the last climatic cycle or extends to sediments deposited prior to the Late Pleistocene, covering a single climatic cycle, we conducted a programme of ESR/U-series combined dating, the results of which are presented in this study.

Materials and methods

We applied the ESR/U-series dating method (Grün *et al.*, 1988) to nine mammal teeth selected from the Middle Palaeolithic faunal assemblages in units S9, S6, S3, BR12-11 and BR9, as well as two teeth from the Proto-Aurignacian unit A2. This study also integrates the first analyses previously conducted on the A11-A4 units (Peresani *et al.*, 2008). Optimal teeth for dating are not available from units BR6 to BR4. In the first phase of the Fumane dating programme, we sampled fragmented herbivore shafts, which however were not optimal samples to apply DATA nor AU/ESR programmes, as the bony tissue systematically exhibited an open uranium uptake system.

To determine the ages, the *U-series model* (US model) combines ESR and U-series data, including radioelement contents, isotopic ratios, equivalent dose and external gamma-dose rates. to reconstruct the uranium uptake history of each dental tissue using a specific U-uptake parameter (p-value) (Grün *et al.*, 1988). Since this model cannot account for uranium loss, an alternative model, the *accelerating uptake model* (AU-ESR) (Shao *et al.*, 2012), was applied to samples showing evidence of slight uranium leaching. The combined use of both models has been successfully applied to date sequences covering the entire Middle Pleistocene, using both human and animal teeth (Grün, 2006; Falguères *et al.*, 2010). A recent study demonstrates the consistency of ESR/U-series dates obtained from herbivorous teeth when compared to other methods, such as $^{40}Ar/^{39}Ar$ of volcanic samples and ESR dating on bleached quartz from Italian sites (Bahain *et al.*, 2021).

We analysed all teeth using combined ESR/U-series at the Geochronology Lab of HNHP, National Museum of Natural History, Paris and at the 'Centre de Spectrochimie' of Paris 6 University. Four samples were collected from the S macro-unit, five from macro unit BR and two from unit A2. All samples consisted of well-preserved premolars from medium-sized cervids or bovids (Fig. 3). Additionally, five previously analysed teeth (from A4 to A11), for which the p parameter had initially been set to −1, were recalculated using data obtained from TL dosimeters inserted in the corresponding units.

Dental tissues (enamel, dentine and for FU0001 tooth cement) were mechanically separated, and their radioisotope contents were measured using U-series alpha-ray spectrometry following standard methods (Bischoff *et al.*, 1988, see details provided in the supplementary information) and gamma-ray spectrometry (Yokoyama and Nguyen, 1980). Enamel was cleaned on both inner and outer surfaces to eliminate the effects of external alpha radiation. It was then ground, sieved at 100–200 µm fraction and split into 10 aliquots. Nine of these aliquots were irradiated with a calibrated ^{60}Co gamma-ray panoramic source (LABRA, CEA, Saclay, France) at doses ranging from 47 to 6000 Gy. ESR measurements were performed on the entire set of aliquots at Paris 6 University using an E-109 X-Band Varian spectrometer (9.82 GHz) for samples labelled FU96. Samples labelled FU00 were analysed at the HNHP lab, MNHN, Paris, using an EMX Bruker spectrometer (X-Band, 9.85 GHz). All measurements were performed at room temperature with a microwave power of 10 mW and a modulation amplitude of 0.1 mT. A scan range of 10 mT, a scan time of 4 min and a modulation frequency of 100 kHz were used for each

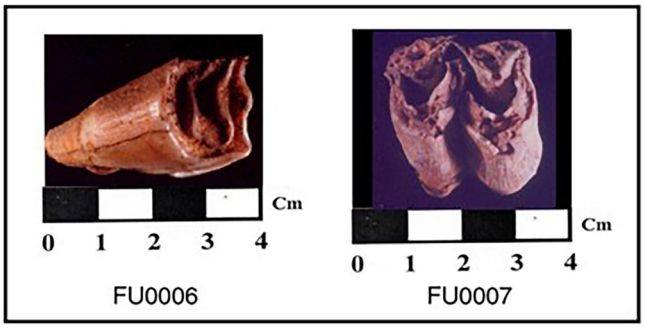

Figure 3. Examples of analysed samples. FU0006 is an inferior bovid molar and FU0007 is a cervid molar, both having a rather thick enamel tissue. [Color figure can be viewed at wileyonlinelibrary.com]

spectrum. Each ESR measurement was repeated three times for each dose over several days. ESR intensities were measured from the asymmetric ESR signal between the T1-B2 peaks at $g = 2.0018$ (Grün *et al.*, 2008). Growth curves were fitted using a single saturating exponential function (SSE) with Origin Pro8 software (Origin Lab Corporation, Northampton, USA) to determine the equivalent dose (D_e) (Figs. S1 and S2). Data were weighted by $1/I^2$.

US-ESR age calculations were carried out using the ESR-DATA program (Grün, 2009), which applies an alpha efficiency of 0.13 ± 0.02 (Grün and Katzenberger-Apel, 1994) and Monte-Carlo beta attenuation factors (Brennan *et al.*, 1997) based on enamel thickness, accounting for the removal of outer layers. Approximately 30% of the samples display $^{234}U/^{238}U$ ratios leading to *p*-values lower than −1 rendering them unsuitable for age calculations using the DATA program. For these samples, which exhibited slight uranium leaching, ages were calculated using the AU-ESR model (Shao *et al.*, 2012). Note that the DATA program derives the dose rate using the conversion factors of Adamiec and Aitken (1998), whereas the AU-ESR program calculates the dose rate using the conversion factors from Guérin *et al.* (2011). Water content was estimated to be $7\% \pm 3\%$ in the dentine and $15\% \pm 5\%$ in sediment (measured as dry weight vs. wet sediment dried in an oven at 35°C). No water content correction was applied to the enamel.

We conducted Gamma-ray spectroscopy measurements using a low-background, high-resolution Ge Ametek© detector to determine the specific activity of radioisotopes (U, Th, K) in the sediments, including those surrounding the samples. To account for the potential loss of Ra and Rn in each tissue, alpha-ray and gamma-ray measurements were combined following the protocol outlined by Bahain *et al.* (1992). To obtain more accurate dosimetry reflecting the heterogeneous sedimentation of cave deposits, 10 TL dosimeters were placed in the studied units in 2005 and retrieved 1 year later (Fig. 2; Table 1). The recorded values provided new estimates for the external dose rates. Among the four dosimeters inserted previously in 1996, three yielded doses comparable to those from the new dosimeters. However, the first dosimeter (DOS1), which was inserted in level A2, was not remeasured. The previously dated teeth were recalculated using the updated values obtained from the 2005 dosimeters.

Results

The ESR/U-series dating results for the Fumane teeth provide new insights into the chronology of the Middle Palaeolithic layers. These results, summarised in Tables 2 and 3, include uranium content, isotopic ratios, equivalent doses (D_e) and dosimetric contributions: key factors in understanding the dating accuracy and the depositional environments conditions. Dates highlighted in red refer to samples from units A11 to A4, as previously reported by Peresani *et al.* (2008). Table 2 presents U content and isotopic ratios for each tissue type across the 16 analysed teeth. Enamel U content ranges from 0.12 to 1.96 ppm, while dentine and cement varied between 11 and 59 ppm. Most isotopic ratios are consistent, except for FU0003, which has a $^{234}U/^{238}U < 1$ in dentine and a $^{230}Th/^{234}U > 1$ in FU9623, both indicative of probable uranium leaching. Table 3 summarises the D_es and the different calculated dosimetric contributions, including external and internal dose components. These contributions incorporate gamma and beta doses measured in the sediment using *in situ* dosimeters and a low-background, high-resolution germanium detector in the laboratory. Cosmic doses were estimated based on the deposit thicknesses and the shelter roof coverage (Prescott and Hutton, 1994). The internal dose includes alpha and beta contributions within the enamel. The data indicate that, for most Fumane teeth, the external dose represents a value ranging between 60% and 93% of the total dose. However, in FU0007 and FU9623, external and internal doses are nearly equal, representing approximately 55% and 45%, respectively. Uranium uptake parameters, detailed in Table 3, are expressed as *p* for the US model (Grün *et al.*, 1988) and *n* for the AU model (Shao *et al.*, 2012).

For the A macro-unit, recalculated ages using the updated dosimetric data generally align with those previously reported by Peresani *et al.* (2008), with the exception for sample FU0004, which yields a younger age due to an internal dose twice as large as that of the other samples, with *p*-values close to −1, corresponding to a minimum age. Samples FU9606 and FU0001 exhibit lower D_e than other samples in the macro-unit A, likely due to complex geochemical behaviour associated with uranium uptake in different dental tissues. For these two teeth, no definitive ages could be calculated using either model, with the indicated age of 32 ± 4 ka corresponding to minimum age in this context. Similarly, sample FU0003 shows evidence of uranium leaching, precluding any reliable age calculation. Samples FU0001 and FU0002 exhibit lower dose rates compared to other macro-unit A samples. The *p* parameters for FU0002 suggest late uranium uptake in dentine and enamel, whereas the *p*-value for FU0001 enamel indicates uranium leaching. This precludes modelling uranium incorporation using the AU model, highlighting the inherent complexity of uranium uptake in these dental tissues.

Table 1. U, Th and K content of the different sediments at the Fumane site.

Sediment layer	U (ppm)	Th (ppm)	K (%)	TL dosimeters (μGy/a)	
A2[a]	2.23 ± 0.08	4.29 ± 0.07	0.64 ± 0.01	Dos 1	291
A4	2.65 ± 0.08	7.60 ± 0.08	1.18 ± 0.01	Dos 14	730
A6	2.51 ± 0.09	6.95 ± 0.08	1.10 ± 0.02	Dos 2	691
A9-A11[a]	$2.68 \pm 0.0.8$	3.22 ± 0.07	0.47 ± 0.01	Dos 13/Dos 12	519/439
BR9[a]	3.27 ± 0.12	6.03 ± 0.10	0.86 ± 0.02	Dos 10	569
BR11[a]	2.77 ± 0.09	4.62 ± 0.07	0.63 ± 0.01	Dos 9	601
BR12[a]	1.91 ± 0.06	2.58 ± 0.04	0.37 ± 0.01	Dos 3	264
S3[b]	1.48 ± 0.08	2.78 ± 0.06	0.47 ± 0.01	Dos 8	204
S6	1.48 ± 0.08	2.78 ± 0.06	0.47 ± 0.01	Dos 7	351
S9[a]	1.41 ± 0.09	3.06 ± 0.07	0.45 ± 0.01	Dos 4/Dos 5	235

TL dosimeter values inserted in each layer during 1 year.
[a] Corresponds to an average of several sediments taken in the same layer.
[b] For the S3 layer, the values obtained for S6 were used.

Table 2. U content and isotopic ratios obtained by alpha-ray spectrometry on the enamel, dentine and cement of each tooth.

		U (ppm)			$^{234}U/^{238}U$			$^{230}Th/^{234}U$				
Sample	Layer	Enamel	Dentine	Cement	Enamel	Dentine	Cement	Enamel	Dentine	Cement	Initial thickness enamel (μm)	dentine/ sediment[a] (μm)
FU0001	A2	0.27 ± 0.03	11.6 ± 1.20	21.45 ± 2.15	1.034 ± 0,096	1.012 ± 0.027	1.024 ± 0.016	0.366 ± 0.062	0.130 ± 0.008	0.214 ± 0.008	1557 ± 156	184/136
FU0002	A2	1.96 ± 0.20	42.45 ± 4.25		1.067 ± 0.050	1.031 ± 0.017		0.090 ± 0.011	0.081 ± 0.004		747 ± 75	96/68
FU0003	A4-1	0.18 ± 0.02	18.23 ± 1.82		1.175 ± 0.095	***0.990 ± 0.028***		0.414 ± 0.041	0.207 ± 0.011		1269 ± 127	93/142
FU9606	A5 + A6	0.24 ± 0.02	14.06 ± 1.41		1.134 ± 0.095	1.041 ± 0.022		0.426 ± 0.042	0.093 ± 0.005		1632 ± 163	100/100
FU9607	A6	0.53 ± 0.05	24.28 ± 2.43		1.113 ± 0.069	1.016 ± 0.027		0.247 ± 0.024	0.215 ± 0.009		1696 ± 170	100/100
FU0004	A9	0.65 ± 0.07	20.56 ± 2.06		1.011 ± 0.133	1.066 ± 0.023		0.506 ± 0.090	0.201 ± 0.010		954 ± 95	116/89
FU0005	A11a	0.12 ± 0.01	17.50 ± 1.75		1.316 ± 0.127	1.069 ± 0.018		0.694 ± 0.074	0.439 ± 0.015		1262 ± 126	102/99
FU0006	BR9	0.7 ± 0.07	14.27 ± 1.43		1.175 ± 0.049	1.096 ± 0.036		0.688 ± 0.035	0.762 ± 0.041		1030 ± 103	192/84
FU0007	BR11b	1.41 ± 0.14	59.33 ± 5.93		1.054 ± 0.035	1.077 ± 0.012		0.417 ± 0.021	0.556 ± 0.016		1037 ± 104	161/75
FU0009	BR11b	0.56 ± 0.06	18.57 ± 0.19		1.031 ± 0.035	1.122 ± 0.029		0.705 ± 0.037	0.830 ± 0.031		888 ± 89	76/100
FU0010	BR11	1.45 ± 0.14	43.99 ± 0.44		1.120 ± 0.054	1.066 ± 0.015		0.458 ± 0.032	0.527 ± 0.017		1064 ± 106	124/92
FU9620	BR12	0.48 ± 0.05	19.50 ± 0.20		1.164 ± 0.067	1.099 ± 0.022		0.734 ± 0.047	0.734 ± 0.019		1440 ± 144	100/100
FU0008	S3	0.55 ± 0.06	22.16 ± 0.22		1.092 ± 0.069	1.066 ± 0.028		0.718 ± 0.057	0.640 ± 0.025		916 ± 92	127/64
FU9621	S6	1.19 ± 0.12	47.00 ± 4.70		1.187 ± 0.031	1.048 ± 0.021		0.483 ± 0.021	0.491 ± 0.016		1440 ± 144	100/100
FU9623	S9	0.46 ± 0.05	16.86 ± 1.69		1.230 ± 0.048	1.386 ± 0.037		***1.106 ± 0.108***	0.720 ± 0.024		1340 ± 134	100/100
FU9624	S9	0.69 ± 0.07	17.16 ± 1.72		1.167 ± 0.036	1.083 ± 0.023		0.976 ± 0.062	0.783 ± 0.022		1340 ± 134	100/100

The samples in bold and italic show anomalous values suggesting uranium uptake complexity.
In bold, the samples already published in Peresani *et al.* (2008).
[a]Thickness subtracted on dentine and sediment or cement side. For teeth of 96, an arbitrary mean value has been taken.

Table 3. D_e in Grays, internal and external contributions and total dose rate, uptake parameters p and n used for age calculations.

Samples	Layer	De (Gy)	(β+γ) sediment and cosmic dose rate (μGy/a)	Internal dose rate (α +β) enamel (μGy/a)	(β) dose rate dentine and cement (μGy/a)	Total dose rate (μGy/a)	Uptake parameters (p and n)			ESR/U-series ages (ka)	ESR/U-series ages (ka)[d]
							Enamel	Dentine	Cement		
FU0001[a]	A2	16.70 ± 0.86	348 ± 30	72 ± 42	104 ± 49	524 ± 71	***−1.25 ± 0.06***	0.06 ± 0.24	−0.77 ± 0.13	32 ± 4	
FU0002	A2	28.90 ± 2.96	475 ± 25	59 ± 50	69 ± 60	603 ± 107	2.42 ± 0.63	2.94 ± 0.71		47 ± 7	
FU0003[b]	A4-1	25.10 ± 0.72	870 ± 41	27 ± 12	98 ± 12	995 ± 48	NC	NC		NC	44 ± 7
FU9606[b]	A5 + A6	17.70 ± 0.53	787 ± 15	32 ± 7	29 ± 6	850 ± 18	NC	NC		NC	38 ± 6
FU9607	A6	37.60 ± 1.28	807 ± 50	64 ± 40	69 ± 44	940 ± 78	−0.72 ± 0.08	−0.52 ± 0.10		40 ± 3	38 ± 6
FU0004[c]	A9	24.50 ± 0.65	678 ± 51	91 ± 39	130 ± 26	899 ± 70	−0.90 ± 0.11	−0.90 ± 0.11		>24	46 ± 7
FU0005[c]	A11a	30.50 ± 0.45	579 ± 22	22 ± 10	107 ± 20	708 ± 32	−0.90 ± 0.05	−0.91 ± 0.05		>39	49 ± 7
FU0006	BR9	132.10 ± 2.02	745 ± 30	153 ± 57	88 ± 33	986 ± 73	−0.93 ± 0.05	*−0.0108 ± 0.0006*		134 ± 9	
FU0007	BR11b	131.10 ± 0.55	744 ± 50	201 ± 52	379 ± 97	1324 ± 121	−0.43 ± 0.12	−0.89 ± 0.08		99 ± 9	
FU0009	BR11b	124.70 ± 6.20	744 ± 50	153 ± 100	302 ± 200	1199 ± 476	*−0.0121 ± 0.0144*	*−0.0058 ± 0.0091*		104 ± 41	
FU0010	BR11	133.50 ± 6.00	736 ± 50	234 ± 138	255 ± 150	1225 ± 210	−0.47 ± 0.19	−0.73 ± 0.15		109 ± 16	
FU9620	BR12	103.60 ± 1.35	331 ± 25	132 ± 41	106 ± 33	569 ± 63	−0.79 ± 0.08	−0.81 ± 0.08		182 ± 18	
FU0008	S3	119.46 ± 4.11	307 ± 25	124 ± 42	117 ± 39	548 ± 63	−0.61 ± 0.10	−0.34 ± 0.14		218 ± 24	
FU9621	S6	102.95 ± 1.72	420 ± 30	194 ± 67	172 ± 59	786 ± 94	−0.33 ± 0.16	−0.38 ± 0.15		131 ± 15	
FU9623	S9	104.85 ± 1.71	306 ± 25	169 ± 43	89 ± 23	564 ± 55	*−0.0082 ± 0.0009*	*−0.0061 ± 0.0010*		186 ± 17	
FU9624	S9	118.06 ± 2.60	451 ± 25	217 ± 64	108 ± 32	776 ± 76	*−0.0094 ± 0.0007*	*−0.0094 ± 0.0008*		152 ± 14	

[a]FU0001 sample shows a strong uranium leaching in the enamel tissue though it was not possible to determine an n parameter.
[b]FU0003 and FU9606 samples cannot yield ages either by US or by AU models when using the new dosimetry!
[c]FU0004 and FU0005 yield minimum ages if we take into account the fact that we are practically under closed conditions without the possibility of applying the AU model.
[d]Ages published previously in Peresani *et al.* (2008) were also recalculated when it was possible.

Most samples from the macro-unit BR yield ages corresponding to MIS5, ranging from 99 to 134 ka for teeth from BR11 and BR9. In contrast, the FU9620 tooth from BR12 presents an older age (182 ± 17 ka). This sample displays an external dose comparable to values obtained in the macro-unit S (Table 1). The uranium, thorium and potassium content in layers from BR12 to the entirety of the macro-unit S are notably lower than those measured in the upper BR layers.

Teeth from macro-unit S present ages between 131 and 218 ka, placing their deposition firmly within MIS7 and MIS6 and indicating a Middle Pleistocene chronology. Notably, the FU9621 tooth from layer S6 contains twice as much uranium in its enamel and dentine compared to other teeth from the unit S. Its younger calculated age likely reflects a complex uranium uptake history, involving an initial phase of incorporation followed by a later uptake during the onset of MIS5. Teeth from unit S9 (FU9623 and FU9624) show evidence of slight uranium leaching, which can be calculated for using the AU model. The resulting minimum age is consistent with an early uranium uptake model, marking the onset of Neanderthal frequentations at Fumane.

Our results for the macro-units BR and S diverge significantly from the TL data previously reported by Martini *et al*. (2001), which suggest ages between 55 ± 7 ka and 79 ± 11 ka. Table 4 highlights the discrepancies between the initial measurements reported in Martini *et al*. (2001) and the gamma dose rates derived from *in situ* analyses and laboratory measurements by gamma spectrometry on ca. 100 g of sediments (this work). Both gamma-based methods yield similar results, with values generally lower than those obtained via alpha counting. The earlier TL findings place the lower part of the Fumane stratigraphic sequence within the Late Pleistocene MIS5b-3 interval (Fig. 4).

The discrepancy appears to stem from differences in the reconstruction of the external dose. Martini *et al*. (2001) used 'ZnS (Ag) scintillators for thick source total alpha counting', a method reliant on measurements of only a few milligrams of fine sediment particles (Peresani *et al*., 2008). This approach is inherently biased, as it focuses on the finest sediment particles, often the most radioactive portion, while excluding the coarser sediment fraction, which may include carbonate clasts that are less radioactive than clay. Furthermore, this method does not account for the dosimetric heterogeneity present in a complex sedimentary sequence such as Fumane. In contrast, the TL dosimeter evaluates a sediment volume of 70 cm in diameter around the dated sample, providing a more representative measure of the gamma dose rate and likely yielding a more reliable external dose for the dated teeth. Moreover, our observations reveal an agreement between *in situ* and laboratory measurements using low-background, high-resolution gamma spectrometry on ca100g sediment samples. These findings suggest that using more representative sediment samples offers a better approximation of the external dose than methods restricted to the finest sediment fraction.

Table 4. Discrepancies between the initial measurements reported in Martini *et al*. (2001) and the gamma dose rates.

Levels	TL samples	De (Gy)	External dose (μGy/a)	Total dose (μGy/a)	Age (ka)
A6	TL1[a]	90 ± 10	730	1780	50 ± 8
	TL1 re[b]		721	1771	51 ± 8
	TL1 resed[c]		721	1771	51 ± 8
BR11	TL2[a]	72 ± 7	459	1310	55 ± 7
	TL2 re[b]		292	1144	63 ± 7
	TL2 resed[c]		426	1278	56 ± 7
BR12	TL3[a]	45 ± 7	672	790	57 ± 8
	TL3 re[b]		292	411	110 ± 15
	TL3 resed[c]		264	383	118 ± 17
S7	TL4[a]	61 ± 7	593	770	79 ± 11
	TL4 re[b]		263	440	139 ± 19
	TL4 resed[c]		259	436	140 ± 20

[a]TL ages calculated in Martini *et al*. (2001).
[b]TL ages are recalculated taking into account the *in situ* dosimetry.
[c]TL ages are recalculated taking into account the gamma lab sediments measurements.

Discussion

Continuity and discontinuity in the stratigraphic sequence

The Fumane sedimentary sequence, previously attributed to the Late Pleistocene based on TL geochronological data, is now confirmed to extend into the latest part of the Middle Pleistocene. This extension begins from unit BR9 and continues downward to unit S9. Unit S9 marks the onset of stratified sedimentary deposition, composing rubble, sand, ecofacts and artefacts. The ESR/U-series dates combined with the recalibrated TL dates of heated flint tools significantly push back the timeline for this portion of the cave infill. This revision is further supported by evidence of sedimentary gaps identified within the sequence excavated during the 1992–1994 campaigns.

The texture, mineralogy and geochemistry of the sub-horizontal layers in the macro-unit S (218-131 ka) are consistent with deposits of dolomite sand, angular stones and surface-weathered boulders. These features reflect moderate roof degradation and the hydrological redistribution of sand grains released through the surface dissolution of the dolomitised bedrock. Cremaschi *et al*. (2005) observed planar red clayey microlaminations in thin sections, which they attributed to clay translocation during soil erosion: a process further supported by peaks in magnetic susceptibility. In the uppermost layers, angular stones increasingly dominate over fine sediments, indicating intensified wall degradation during a cool climatic trend. Cold conditions are broadly indicated by the higher frequency of ibex and chamois remains relative to cervids, particularly in units S9 and S3, despite the limited number of specimens (Fiore *et al*., 2004). However, additional data from small mammals or birds is currently unavailable, preventing a biochronological confirmation of the placement of units S6 to S9 within a cold isotopic stage.

The overlying macro-unit BR (99–182 ka) rests in paraconformity over the underlying layers. BR is a massive sedimentary body composed of stones and aeolian dust, with frost shattering identified as the dominant sedimentary process throughout the macro-unit. This process is particularly evident in the coarse open-work breccia of the undated units BR5 and BR4, which contain a Quina industry. The fine fraction varies in composition, replacing the sandy dolomitic component. Its aeolian provenance is attested by high levels of magnetic susceptibility (SM) and residual anisteretic magnetisation (RAM), indicative of a higher concentration of heavy minerals such as amphiboles, pyroxenes and garnets, compared to dolomite, quartz and feldspars (Cremaschi *et al*., 2005).

At the micromorphological scale, ice-lensing-related microstructure has been observed (Cremaschi *et al*., 2005). Environmental and climatic interpretation suggests that unit BR formed during a glacial period with humid pulses, particularly in BR11 and BR7, where carbonate deposition occurred. The combination

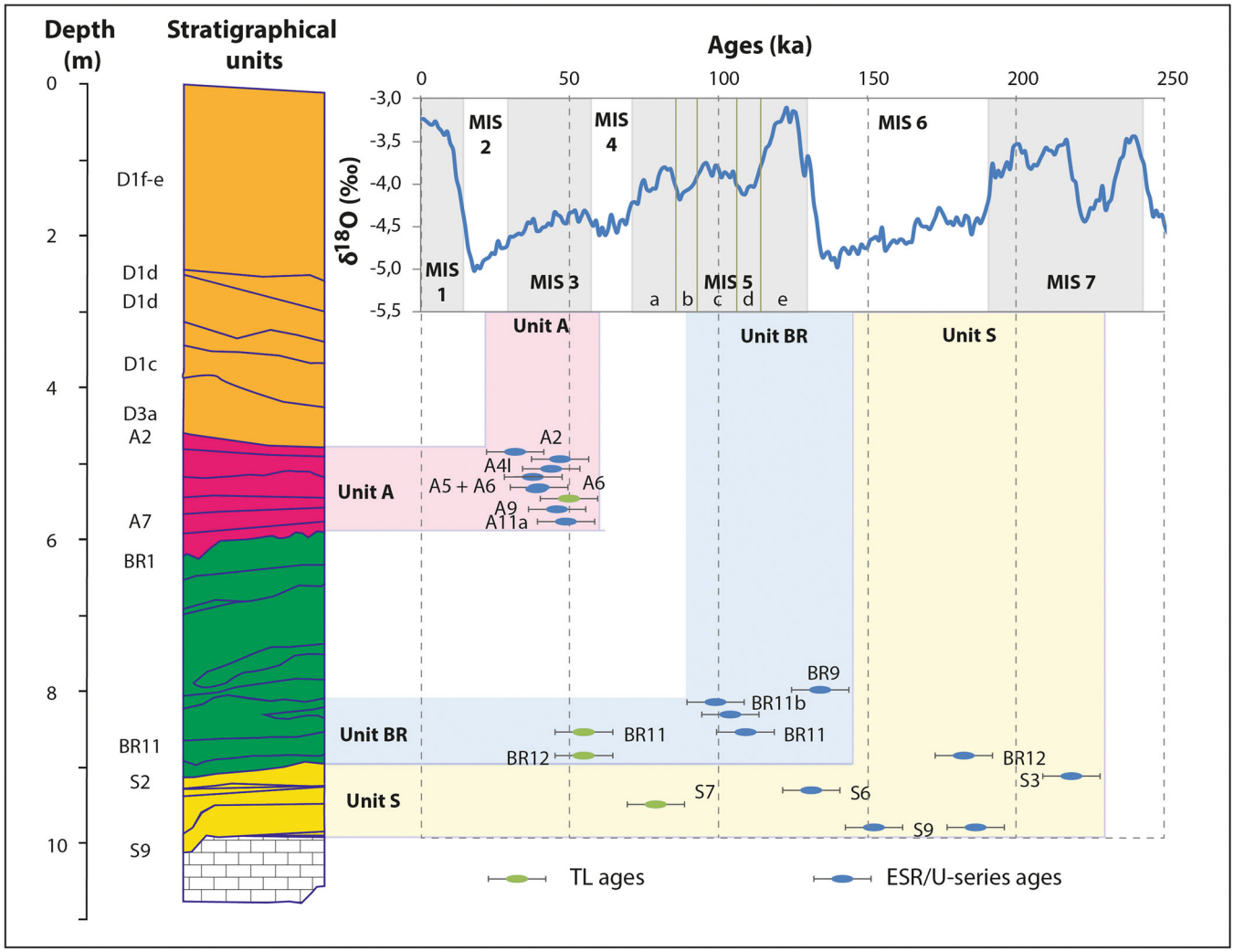

Figure 4. Location of the analysed samples versus marine isotope stages (Lisiecki and Raymo, 2005). The blue ellipses in units A, BR and S correspond to ESR/U-series ages. The green ellipses are TL ages from Martini *et al.* (2001). All the error ranges are given with 1 sigma. [Color figure can be viewed at wileyonlinelibrary.com]

of features—including the high sedimentation rate, in BR5-BR4, and the apparent lack of post-depositional alterations—point to intense cryogenic activity during cold climate conditions (Cremaschi *et al.*, 2005). ESR/U-series dating confirms that aeolian sedimentation in Northern Italy occurred not only from MIS4 onwards but also in earlier periods (Costantini *et al.*, 2018). These environmental conditions are further reflected in the archaeofaunal assemblages. While cervids dominate the initial phases up to BR7, the transition from BR6 to BR1 reveals a shift toward caprids and megacervids, peaking in BR1. This shift, alongside the reduced presence of cervids and bovids, is correspective of a climatic transition to colder and drier conditions (Fiore *et al.*, 2004).

This discontinuity can be further refined by considering the cultural attribution of units BR6 to BR3 to the Quina Mousterian (Peresani, 2012). Recent studies suggest that units BR5 to BR3 exhibit strong similarities with Quina reduction methods and techno-functional layouts observed in Middle Palaeolithic contexts of Western Europe, offering opportunities for large-scale comparisons across Europe (Peresani *et al.*, 2023). Furthermore, an ongoing study on the lithic industry from unit BR6 reinforces its affinity with the Quina system. Although units BR6 to BR3 remain undated, their chronological position is inferred to fall within MIS4 up to early MIS3, based on cultural affinities with analogous assemblages including those from a regional scale, such as De Nadale cave, dated to MIS4 (Delpiano *et al.*, 2022), and Ghiacciaia Cave, which remains undated (Peresani *et al.*, 2022). Across Europe, numerous sites exhibiting similar characteristics are dated to the same period, particularly in Western Europe (see Delpiano *et al.*, 2022 and references therein).

If our cultural correlations suggest a Late Pleistocene age for the Quina contexts, it can be hypothesised that the sediments of BR7, serving as the substrate for the initial Quina Neanderthal occupations in BR6, as evidenced by fireplaces, scattered bones and stone tools (Cremaschi et al., 2002), likely date to the Late Middle Pleistocene. Indeed, a prominent lithological discontinuity is evident in the stratigraphic section, where the homogeneity, texture and compactness of BR7 contrast with the fresh frost-shattered rubble of BR5 and BR4. Furthermore, deep geophysical surveys of the cave fill have revealed this discontinuity as a marked boundary, in addition to another significant boundary at the top of macro-unit BR, coinciding with BR1 in the main sagittal section (Abu Zeid *et al.*, 2019).

The preliminary nature of the 1992–1994 test pit prevents further assessment of the spatial extent of this discontinuity. It also precludes confirmation of its temporal range, which is tentatively constrained between MIS4, serving as the *terminus ante-quem* based on the Quina assemblages, and the MIS5 *terminus post-quem*, represented by the most recent date of unit BR9 (125 ka, as shown in the Table 3). Currently, no conclusive evidence identifies the post-depositional process (es) responsible for potential erosional phases or for a

reduction or cessation of sediment aggradation. While field observations and partial geochemical data reveal no weathered sediments, this does not rule out the possibility of decreased aggradation during much of MIS 5.

If the BR9 date is confirmed through further advancements in the chronometric framework of the Fumane deposits, the representativity of the BR8–BR7 sediments within the original cave system must be reconsidered. According to these dates, the high sedimentation rate of BR9-BR7 would have occurred during MIS5, inconsistent with typical cave entrance environments. Sedimentation dominated by rock collapse and frost-shattered stones is generally associated with cold climatic conditions, rather than warmer or temperate conditions of interglacial periods, despite the cooler oscillations of MIS 5d and MIS 5b. However, during this period, the cave was likely more extensive than it is today, suggesting that the sediments under study represent an inner area of the cave. The absence of Middle Pleistocene cave deposits investigated in the Monti Lessini region poses significant challenges for contextualising Fumane and hinders efforts to reconstruct the evolution of the cave and its sedimentary dynamics.

For macro-unit A (32–49 ka), the transition between Mousterian (A5-A4), Uluzzian (A3) and proto-Aurignacian levels (A2) has been previously radiocarbon dated using charcoal and bone samples, further supported by Bayesian modelling (Higham *et al.*, 2014; Marín-Arroyo *et al.*, 2023). Findings from Higham *et al.* (2014) suggest that the end of the Mousterian occurred between 41 and 39 ka. Our ESR/U-series data align with this range (Peresani *et al.*, 2008), although the large error margin highlights the inherent challenges of applying the ESR/U-series method to fossil enamel for samples younger than 50 ka (Richard *et al.*, 2017). The youngest samples analysed (unit A) are characterised by low D_e, ranging from 17 to 38 Gy, and low uranium content (0.12 to 0.65 ppm, with the exception of sample FU0002). Additionally, the external dose rate (sediments and cosmic doses) represents between 66% and 93% of the total dose rate received by these samples, rendering the calculation of precise ages particularly challenging, if not feasible.

Fumane and the early Middle Palaeolithic sequence in Italy

Fumane cave lies in a geographic district around the Northern Adriatic Sea, including the Eastern Alps, Dalmatian coast and Northern Apennines. Within this region, Neandertals exhibited a range of cultural traits, particularly evident in lithic assemblages characterised by the systematic application of the Levallois method (Karavanić, 2004; Peresani, 2011; Peresani *et al.*, 2014; Karavanić *et al.*, 2022; Romagnoli *et al.*, 2022). At Fumane, the Levallois method is first observed in the lowermost units, beginning with unit S9, where recurrent centripetal Levallois flakes and single unipolar core define a cultural assemblage that includes tools such as simple, biconvex, convergent and thinned scrapers shaped on long Levallois blanks and ordinary flakes. The prevalence of Levallois technology continues into unit S6, where centripetal and unipolar cores with moderate preparation of core convexities were used to produce thin regular blanks, some of which were shaped into side-scrapers. In unit S3, the technological patterns reveal dominance of recurrent unipolar reduction sequences over other modalities. The degree of predetermination varies from moderate to expedient, with core lateral–distal convexities shaped expediently. Tools from this unit primarily include scrapers—lateral, bilateral and convergent—with evidence of recycled fragmentary flakes. The continuity of the extensive application of Levallois technology is further confirmed in unit BR12, where unipolar recurrent modalities dominate, particularly during the earlier phases, while centripetal reduction often appears in the final stages of the sequence. Core convexities were maintained with a moderate to low degree of predetermination, with only a limited number of preparatory flakes used to facilitate serial production of elongated blanks. The tools are mostly side scrapers, as well as points and denticulates, with minimal heavy retouching cycles observed.

In the dense palimpsest of unit BR11, the Levallois production is structured around a main reduction sequence using recurrent unipolar exploitation, accompanied by secondary reduction sequences. Technical variants include a unidirectional modality, consisting of convergent unidirectional detachments or variably oriented removals. Lateral convexities were maintained through ordinary and Levallois core-edge removal flakes, while distal convexities were maintained through diverse techniques. The centripetal modality plays a secondary role, often activated during the middle and final stages of the unidirectional sequence in response to changing knapping constraints. The Mousterian context of unit BR11 is further enriched by a diverse tool assemblage, including scrapers produced on elongated Levallois flakes, as well as points, notches, denticulates and flakes with ventral thinning (Peresani, 2012).

To summarise, Levallois production at the Fumane Cave involves two recurrent modalities: unidirectional and centripetal. The unidirectional modality was applied throughout the later stages of the reduction sequence, focusing on the production of elongated blanks with thin, regular edges, which were often suitable for retouching (Peresani, 2012). This dual-purpose approach explains the observed shifts in core exploitation patterns, including a series of convergent or orthogonal detachments, designed to reduce flint wastage during the reshaping of core-face convexities. In contrast, the centripetal modality was systematically employed, particularly in the final stages of the core reduction or during the exploitation of flake cores. This technological shift aimed to reduce the frequency of core-face reshaping operations while increasing the production of predetermined blanks, albeit at the expense of maintaining morphotechnical properties. When the size of elongated blanks dropped below a functional threshold, the centripetal approach optimised resource economy by facilitating the removal of accidental features, ensuring efficient use of the remaining flint.

The emergence of Levallois industries at Fumane represents one of the earliest chronological instances of this technology in the subalpine region. A comparable chronological pattern of occupation is observed in units VIII and VII of the stratigraphical sequence at the San Bernardino cave, located approximately 70 km east of Fumane, where recurrent centripetal and unipolar Levallois technologies were used (Picin *et al.*, 2013).

On a broader scale across Italy, Levallois was the dominant knapping method at most early Middle Palaeolithic sites, despite regional variations in geomorphology, ecology and raw material availability. The earliest recorded appearance of Levallois in Italy is in the Aniene river basin in central Latium. Deposits at the site of Sedia del Diavolo (Taschini, 1967) and Monte delle Gioie (Taschini, 1967) have been chronostratigraphically dated between 295 and 290 ka (Soriano and Villa, 2017), placing them among the oldest in Europe and preceding the Levallois industry of layer d at Torre in Pietra (Villa *et al.*, 2016), northwest of Rome. At Sedia del Diavolo and Monte delle Gioie, Levallois debitage is featured by recurrent centripetal exploitation and is contextualised within an original technical context, distinct from other early appearances of Levallois. Middle Palaeolithic technology including Levallois is securely attested in Emilia-Romagna at Cave dall'Olio, where deposits are presumed to date as far back as MIS9-MIS8, although direct dating of the thick fluvial

terrace embedding these findings remains unavailable (Fontana *et al.*, 2013). Incertitude surrounds the site of Guado San Nicola in Southern Italy (Peretto *et al.*, 2016), where Levallois technology has been reported as early as late MIS11 within an Acheulian industry, potentially backdating its appearance in Western Europe. However, challenges in identifying early Levallois technology have been highlighted by Soriano and Villa (2017), who argue that some purported Levallois cores lack fundamental technological criteria. They propose reclassifying these as simpler centripetal debitage systems, characterised by two hierarchically organised surfaces, rather than true Levallois cores.

Beyond these Italian contexts, several Western European sites provide convincing evidence for the emergence of Levallois technology between the end of MIS9 and the early MIS8, or earlier as supposed by Moncel *et al.* (2020). These sites express a variety of methods and associations with other lithic products. In Southern Europe, Orgnac 3 in the Rhône Valley dated to 275 ka, documents the progressive adoption of Levallois, culminating at the top of the sequence around 230 ka (Bahain *et al.*, 2022), while in Northern France, it was observed occasionally at Cagny la Garenne and Cagny Ferme de l'Epinette since at least at 400–450 ka (Lamotte and Tuffreau, 2016) (Fig. 5). Similarly, recurrent centripetal Levallois debitage features the assemblage at Kesselt Op-de-Schans (Belgium) during the transition from MIS9 to MIS8 (Van Baelen *et al.*, 2008). In France, at Les Bosses, centripetal Levallois products are found alongside other flake technologies, bifaces and large cutting tools, dating to around 300 ka (Jarry *et al.*, 2007). Conversely, at Purfleet, England, centripete Levallois cores have been observed. Again in England, at Baker's Hole, preferential and recurrent Levallois debitage, dated to MIS8 and MIS 7, appears without any associated biface production (Scott *et al.*, 2010). In Southwestern France, level 2 of Petit Bost (Hérisson *et al.*, 2016), dated to MIS 9/MIS 8, exhibits Levallois debitage with recurrent parallel unipolar or bipolar flake removals, accompanied by a small number of handaxes.

Similar variability in the earliest Levallois techno-complexes is evident throughout the late Middle Pleistocene in Italy. This is exemplified by the cultural assemblage of unit BR9, which includes a few bifaces, unipolar and centripetal Levallois flakes and retouched flakes. Among the bifaces, one hand axe was extensively shaped, while another remained in a rough, unfinished state. A third biface, found in a fragmentary condition, was too incomplete for a full diagnosis. Although no flakes directly associated with bifacial manufacture were recovered, the lithological and taphonomic features of these artefacts align well with the overall assemblage. Compared to the units described above, BR9 records a higher incidence of the exploitation of large flake cores, often involving more intricate preparations aimed at producing flake blades. The tool assemblage primarily comprises scrapers and some points, made on Levallois flakes. However, flake production does not preclude the use of ephemeral methods to produce flakes of variable shape and thickness from mono- and multidirectional cores (Peresani, 2012).

The recovery of bifaces in the North Adriatic region has been documented in the Monti Lessini, where loess-like deposits, palaeosols and reworked sediments containing bifaces and other artefacts are preserved under different contextual conditions, such as sinkholes, ground depressions and grikes. While some sites are located on valley floors, the majority are distributed at mid-elevation along slopes and on ridge tops (Margaritora *et al.*, 2020). These finds are extremely challenging to date due to extensive post-depositional weathering, which has significantly altered the archaeological contexts and caused surface patination of the artefacts. Notable sites such as Quinzano,

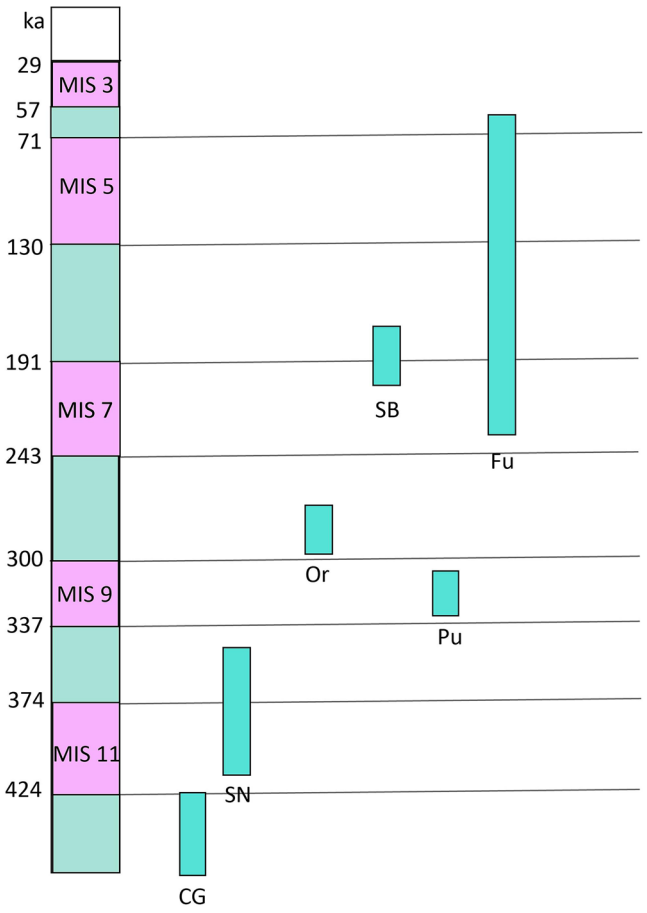

Figure 5. Chronological sketch of the Levallois technique of different French, Italian and English sites in which the Levallois technique has been used versus marine isotopic stages (Lisiecki and Raymo, 2005). CG is Cagny-la-Garenne, France, dated to 400–450 ka by ESR on quartz (Antoine *et al.*, 2003; Lamotte and Tuffreau, 2016). SN is Guado San Nicola, Italy, dated to 350 and 400 ka by $^{40}Ar/^{39}Ar$ on volcanic minerals and by a mean age of 364 ka obtained on six herbivorous teeth by ESR/U-series (Peretto *et al.*, 2016). Or is Orgnac3, France, dated by a multi-method approach to around 275 ka for the human bearing levels in which Levallois technology appears (Bahain *et al.*, 2021). Pu is Purfleet, England, dated to 320 ka by the ESR/U-series on a herbivorous tooth (Voinchet *et al.*, 2015) including Levallois assemblage in the upper part of the stratigraphy (Schreve *et al.*, 2002). SB is San Bernardino, Italy, dated by ESR/U-series on bones and teeth to around 180 ka (mean age) (Picin *et al.*, 2013). Fu is Fumane in this work. [Color figure can be viewed at wileyonlinelibrary.com]

Monte Gazzo and Cà Palui exhibit Levallois artefacts in association with bifaces. Quinzano remains the most important pedo-sedimentological reference for understanding the geomorphological evolution of the landscape at the foot of the Lessini. The sequence contains associations with faunal remains of deer, elephant, fallow deer and roe deer (Zorzi and Pasa, 1945; Pasa 1956), but it is currently inaccessible for sampling and dating. The Lower and Middle Palaeolithic levels are embedded in the lowermost macro-unit (Unit 1, Cremaschi, 1984), comprising alternating palaeosols and slope-waste deposits, separated by erosional surfaces with stone lines. Further evidence for the bifaces associated with Levallois industries is also found at sites along the southern edge of the Po plain, particularly on the terraces along the northern slope of the Appennini, such as Cave dall'Oglio. Similar industries extend along the Adriatic coastal belt down to the Marche region, with attestation no later than MIS5e, based on geomorphological, sedimentological and faunal evidence at Boccabianca (Silvestrini *et al.*,2001).

Conclusions

Our ESR/U-series analysis on teeth suggests that the Middle Palaeolithic sequence of Fumane Cave spans the late Middle Pleistocene and the Late Pleistocene, corresponding to a period covering at least two climatic cycles, from MIS7-6 to MIS5-4, rather than being confined to a single cycle as previously suggested by TL dating results (Martini *et al.*, 2001). Discrepancies between these two sets of dates—both relying on trapped-charge techniques and similar palaeodosimetric approaches—appear to stem primarily from differences in external dose rate determination. This represents indeed the main part of the dose rate received by the dated samples, and the doses measured *in situ* by TL dosimeters or derived from 100 g lab gamma spectrometry analyses differ significantly from those derived using thick-source total alpha counting.

Refining the geochronological framework at Fumane is crucial for advancing our understanding of Neanderthal lithic behaviours, particularly within the broader context of Western Eurasia. Continuous improvements in dating techniques remain essential for accurately situating Middle and Late Pleistocene human occupations in their environmental and cultural contexts.

Acknowledgements. Research at Fumane is coordinated by the Ferrara University in the framework of a project supported by the Ministry of Culture—Veneto Archaeological Superintendency, public institutions (Lessinia Regional Natural Park, Fumane Municipality) and private associations and companies. ESR and U-series analyses were performed during the PhD of Giulia Gruppioni. The authors acknowledge Bernard Morin for his support in the ESR measurements and Theppa Mudiyanselage Kalangi Irushika Rodrigo for revising language and grammar. Open access publishing facilitated by Universita degli Studi di Ferrara, as part of the Wiley – CRUI-CARE agreement.

Data Availability Statement

The data that support the findings of this study are available from the corresponding author upon reasonable request.

Supporting information

Additional supporting information may be found in the online version of this article at the publisher's website.

Figure S1. Growth curves of the enamel samples of Fumane cave calculated by using the SSE function.

Figure S2. Growth curves of the enamel samples of Fumane cave calculated by using the SSE function.

References

Abu Zeid, N., Bignardi, S., Russo, P. & Peresani, M. (2019) Deep in a Paleolithic archive: integrated geophysical investigations and laser-scanner reconstruction at Fumane Cave, Italy. *Journal of Archaeological Science: Reports*, 27, 101976. Available from: https://doi.org/10.1016/j.jasrep.2019.101976

Adamiec, G. & Aitken, M.J. (1998) Dose-rate conversion factors: update. *Ancient TL*, 16, 37–50.

Antoine, P., Limondin-Lozouet, N., Auguste, P., Lamotte, A., Bahain, J.-J., Falguères, C. *et al.* (2003) Paléoenvironnements pléistocènes et peuplements paléolithiques dans le bassin de la Somme (nord de la France). *Bulletin de la Société préhistorique française*, 100, 5–28. Available from: https://doi.org/10.3406/bspf.2003.12790

Bahain, J.-J., Mercier, N., Valladas, H., Falguères, C., Masaoudi, H., Joron, J.-L. *et al.* (2022) Reappraisal of the chronology of Orgnac 3 Lower-to-Middle Paleolithic site (Ardèche, France), a regional key sequence for the Middle Pleistocene of southern France. *Journal of Human Evolution*, 162, 103092. Available from: https://doi.org/10.1016/j.jhevol.2021.103092

Bahain, J.J., Voinchet, P., Vietti, A., Shao, Q., Tombret, O., Pereira, A. *et al.* (2021) ESR/U-series and ESR dating of several Middle Pleistocene Italian sites: comparison with 40Ar/39Ar chronology. *Quaternary Geochronology*, 63, 101151. Available from: https://doi.org/10.1016/j.quageo.2021.101151

Bahain, J.-J., Yokoyama, Y., Falguères, C. & Sarcia, M.N. (1992) ESR dating of tooth enamel: a comparison with K/Ar dating. *Quaternary Science Reviews*, 11, 245–250. Available from: https://doi.org/10.1016/0277-3791(92)90069-K

Bischoff, J.L., Rosenbauer, R.J., Tavoso, A. & de Lumley, H. (1988) A test of uranium-series dating of fossil tooth enamel: results from Tournal Cave, France. *Applied Geochemistry*, 3, 145–151. Available from: https://doi.org/10.1016/0883-2927(88)90002-9

Brennan, B.J., Rink, W.J., McGuirl, E.L., Schwarcz, H.P. & Prestwich, W.V. (1997) Beta doses in tooth enamel by "one-group" theory and the ROSY ESR dating software. *Radiation Measurements*, 27, 307–314. Available from: https://doi.org/10.1016/S1350-4487(96)00132-1

Costantini, E.A.C., Carnicelli, S., Sauer, D., Priori, S., Andreetta, A., Kadereit, A. *et al.* (2018) Loess in Italy: genesis, characteristics and occurrence. *Catena*, 168, 14–33. Available from: https://doi.org/10.1016/j.catena.2018.02.002

Cremaschi, M. (1984) I paleosuoli ed i depositi atriali delle cavità carsiche e dei ripari. In: Aspes, A. (Ed.) *Il Veneto Nell'antichità*. Verona: Banca Popolare di Verona, pp. 101–113.

Cremaschi, M., Ferraro, F., Peresani, M. & Tagliacozzo, A. (2005) Il sito: nuovi contributi sulla stratigrafia, la cronologia, le faune a macromammiferi e le industrie del paleolitico antico. In: Broglio, A. & Dalmeri, G. (Eds.) *Pitture Paleolitiche Nelle Prealpi Venete: Grotta Di Fumane e Riparo Dalmeri, Atti Del Simposio, Memorie Museo Civico Di Storia Naturale Di Verona, 2. Serie, Sezione Scienze Dell'Uomo*. Italy: Museo delle Scienze, pp. 12–22.

Cremaschi, M., Peresani, M. & Pizziolo, G. (2002) Analisi spaziale del suolo d'abitato musteriano BR6base della Grotta di Fumane. In: Peretto, C. (Ed.) *Analisi Informatizzata e Trattamento Dati Delle Strutture Di Abitato Di Età Preistorica e Protostorica in Italia*. Italy: Istituto Italiano di Preistoria e Protostoria, pp. 59–70.

Delpiano, D., Zupancich, A., Bertola, S., Martellotta, E.F., Livraghi, A., Cristiani, E. *et al.* (2022) Flexibility within Quina lithic production systems and tool-use in Northern Italy: implications on Neanderthal behavior and ecology during early MIS 4. *Archaeological and Anthropological Sciences*, 14, 219. Available from: https://doi.org/10.1007/s12520-022-01684-2

Douka, K., Higham, T.F.G., Wood, R., Boscato, P., Gambassini, P., Karkanas, P. *et al.* (2014) On the chronology of the Uluzzian. *Journal of Human Evolution*, 68, 1–13. Available from: https://doi.org/10.1016/j.jhevol.2013.12.007

Falcucci, A. & Peresani, M. (2019) A pre-Heinrich Event 3 assemblage at Fumane Cave and its contribution for understanding the beginning of the Gravettian in Italy. *Quartar International Yearbook for Ice Age and Stone Age Research*, 66, 135–154. Available from: https://doi.org/10.7485/QU66_6

Falcucci, A., Conard, N.J. & Peresani, M. (2020) Breaking through the aquitaine frame: a re-evaluation on the significance of regional variants during the Aurignacian as seen from a key record in southern Europe. *Journal of anthropological sciences = Rivista di antropologia: JASS*, 98, 99–140. Available from: https://doi.org/10.4436/jass.98021

Falguères, C., Bahain, J.-J., Duval, M., Shao, Q., Han, F., Lebon, M. *et al.* (2010) A 300–600ka ESR/U-series chronology of Acheulian sites in Western Europe. *Quaternary International*, 223–224, 293–298. Available from: https://doi.org/10.1016/j.quaint.2009.10.008

Fiore, I., Gala, M. & Tagliacozzo, A. (2004) Ecology and subsistence strategies in the Eastern Italian Alps during the Middle Palaeolithic. *International Journal of Osteoarchaeology*, 14, 273–286. Available from: https://doi.org/10.1002/oa.761

Fontana, F., Moncel, M.-H., Nenzioni, G., Onorevoli, G., Peretto, C. & Combier, J. (2013) Widespread diffusion of technical innovations around 300,000 years ago in Europe as a reflection of anthropological and social transformations? New comparative data from the western Mediterranean sites of Orgnac (France) and Cave

dall'Olio (Italy). *Journal of Anthropological Archaeology*, 32, 478–498. Available from: https://doi.org/10.1016/j.jaa.2013.08.003

Grün, R. (2006) Direct dating of human fossils. *American Journal of Physical Anthropology*, 131, 2–48. Available from: https://doi.org/10.1002/ajpa.20516

Grün, R. (2009) The DATA program for the calculation of ESR age estimates on tooth enamel. *Quaternary Geochronology*, 4, 231–232. Available from: https://doi.org/10.1016/j.quageo.2008.12.005

Grün, R. & Katzenberger-Appel, O. (1994) Alpha irradiator for ESR dating. *Ancient TL*, 12, 35–38.

Grün, R., Joannes-Boyau, R. & Stringer, C. (2008) Two types of CO_2-radicals threaten the fundamentals of ESR dating of tooth enamel. *Quaternary Geochronology*, 3, 150–172. Available from: https://doi.org/10.1016/j.quageo.2007.09.004

Grün, R., Schwarcz, H.P. & Chadam, J. (1988) ESR dating of tooth enamel: coupled correction for U-uptake and U-series disequilibrium. *International Journal of Radiation Applications and Instrumentation. Part D*, 14, 237–241. Available from: https://doi.org/10.1016/1359-0189(88)90071-4

Gruppioni, G., (2004) Datation par les méthodes uranium-thorium (U-Th) et résonance paramagnétique électronique (RPE) de deux gisements du Paléolithique moyen et supérieur de Vénétie: la grotte de Fumane (Monts Lessini, Vérone) et la grotte majeure de San Bernardino (Monts Berici, Vicence). PhD dissertation, University of Ferrara, 174 pp.

Guérin, G., Mercier, N. & Adamiec, G. (2011) Dose-rate conversion factors: update. *Ancient TL*, 29, 5–8.

Hérisson, D., Brenet, M., Cliquet, D., Moncel, M.H., Richter, J., Scott, B. *et al*. (2016) The emergence of the Middle Palaeolithic in north-western Europe and its southern fringes. *Quaternary International*, 411, A 233–283. Available from: https://doi.org/10.1016/j.quaint.2016.02.049

Higham, T., Brock, F., Peresani, M., Broglio, A., Wood, R. & Douka, K. (2009) Problems with radiocarbon dating the Middle to Upper Palaeolithic transition in Italy. *Quaternary Science Reviews*, 28, 1257–1267. Available from: https://doi.org/10.1016/j.quascirev.2008.12.018

Higham, T., Douka, K., Wood, R., Ramsey, C.B., Brock, F., Basell, L. *et al*. (2014) The timing and spatiotemporal patterning of Neanderthal disappearance. *Nature*, 512, 306–309. Available from: https://doi.org/10.1038/nature13621

Jarry, M., Colonge, D., Lelouvier, L.A. & Mourre, V. (2007) Les Bosses 1, Lamagdelaine (Lot): un gisement paléolithique moyen antérieur à l'avant-dernier Interglaciaire sur la moyenne terrasse du Lot. *Société Préhistorique Française*, 7, 158.

Karavanić, I. (2004) The Middle Paleolithic Settlement of Croatia. In: *Settlement Dynamics of the Middle Paleolithic and Middle Stone Age*, II. Tübingen: Kerns Verlag.

Karavanić, I., Banda, M., Radović, S., Miko, S., Vukosavljević, N., Razum, I. *et al*. (2022) A palaeoecological view of the last Neanderthals at the crossroads of south-central Europe and the central Mediterranean: long-term stability or pronounced environmental change with human responses. *Journal of Quaternary Science*, 37, 194–203. Available from: https://doi.org/10.1002/jqs.3279

Kehl, M., Marcazzan, D., Miller, C.E., Falcucci, A., Duches, R. & Peresani, M. (2025) The upper sedimentary sequence of Grotta di Fumane, Northern Italy: a micromorphological approach to study imprints of human occupation and paleoclimate change. *Geoarchaeology*, 40, e70000.

Lamotte, A. & Tuffreau, A. (2016) Acheulean of the Somme basin (France): assessment of lithic changes during MIS 12 to 9. *Quaternary International*, 409, 54–72.

Lisiecki, L.E. & Raymo, M.E. (2005) A Pliocene-Pleistocene stack of 57 globally distributed benthic stable oxygen isotope records. *Paleoceanography*, 20, PA1003.

Margaritora, D., Dozio, A., Chelidonio, G., Turrini, M.C. & Peresani, M. (2020) The Lower and Middle palaeolithic settlements in the Baldo-Lessini mountains. Results from a GIS investigation. *Alpine and Mediterranean Quaternary*, 33, 115–132. Available from: https://doi.org/10.26382/AMQ.2020.13

Marín-Arroyo, A.B., Terlato, G., Vidal-Cordasco, M. & Peresani, M. (2023) Subsistence of early anatomically modern humans in Europe as evidenced in the Protoaurignacian occupations of Fumane Cave, Italy. *Scientific Reports*, 13, 3788. Available from: https://doi.org/10.1038/s41598-023-30059-3

Martini, M., Sibilia, E., Croci, S. & Cremaschi, M. (2001) Thermoluminescence (TL) dating of burnt flints: problems, perspectives and some examples of application. *Journal of Cultural Heritage*, 2, 179–190. Available from: https://doi.org/10.1016/S1296-2074(01)01126-8

Moncel, M.H., Ashton, N., Arzarello, M., Fontana, F., Lamotte, A., Scott, B. *et al*. (2020) Early Levallois core technology between Marine Isotope Stage 12 and 9 in Western Europe. *Journal of Human Evolution*, 139, 102735. Available from: https://doi.org/10.1016/j.jhevol.2019.102735

Pasa, A. (1956) Nuovi indici paleoclimatici dal deposito di Quinzano veronese. *Atti Accademia Agricoltura, Scienze & Lettere di Verona, Serie VI, Vol. VI*, pp. 39–60.

Peresani, M. (2011) The end of the Middle Palaeolithic in the Italian Alps. An overview on Neandertal land-use, subsistence and technology. In: Conard, N. & Richter, J.(Eds.) *Neanderthal lifeways, subsistence and technology. One hundred fifty years of neanderthal study*. Vertebrate Paleobiology and Paleoanthropology Series. Dordrecht: Springer, pp. 249–259. Available from: https://doi.org/10.1007/978-94-007-0415-2_21

Peresani, M. (2012) Fifty thousand years of flint knapping and tool shaping across the Mousterian and Uluzzian sequence of Fumane cave. *Quaternary International*, 247, 125–150. Available from: https://doi.org/10.1016/j.quaint.2011.02.006

Peresani, M. (2022) Inspecting human evolution from a cave. Late Neanderthals and early sapiens at Grotta di Fumane: present state and outlook. *Journal of Anthropological Sciences*, 100, 71–107. Available from: https://doi.org/10.4436/jass.10016

Peresani, M., Bourguignon, L., Delpiano, D. & Lemorini, C. (2023) Quina on the edge. Insights from a Middle Palaeolithic lithic assemblage of Grotta di Fumane, Italy. *Journal of Archaeological Science: Reports*, 49, 103998. Available from: https://doi.org/10.1016/j.jasrep.2023.103998

Peresani, M., Cremaschi, M., Ferraro, F., Falguères, C., Bahain, J.J., Gruppioni, G. *et al*. (2008) Age of the final Middle Palaeolithic and Uluzzian levels at Fumane Cave, Northern Italy, using 14C, ESR, 234U/230Th and thermoluminescence methods. *Journal of Archaeological Science*, 35, 2986–2996. Available from: https://doi.org/10.1016/j.jas.2008.06.013

Peresani, M., Hohenstein, U.T., Delpiano, D., De Lorenzi, M., Rio, M. & Del, M. *et al*. (2022) Grotta della Ghiacciaia. Ripresa delle indagini su un sito del Paleolitico Medio e Superiore in Lessinia. *Preistoria Alpina*, 52, 47–61.

Peresani, M., Romandini, M., Duches, R., Jéquier, C., Nannini, N., Pastoors, A. *et al*. (2014) New evidence for the Mousterian and Gravettian at Rio Secco Cave, Italy. *Journal of Field Archaeology*, 39, 401–416.

Peretto, C., Arzarello, M., Bahain, J.J., Boulbes, N., Dolo, J.M., Douville, E. *et al*. (2016) The Middle Pleistocene site of Guado San Nicola (Monteroduni, Central Italy) on the Lower/Middle Palaeolithic transition. *Quaternary International*, 411, 301–315. Available from: https://doi.org/10.1016/j.quaint.2015.11.056

Picin, A., Peresani, M., Falguères, C., Gruppioni, G. & Bahain, J.J. (2013) San Bernardino Cave (Italy) and the appearance of Levallois technology in Europe: results of a radiometric and technological reassessment. *PLoS One*, 8, e76182. Available from: https://doi.org/10.1371/journal.pone.0076182

Prescott, J.R. & Hutton, J.T. (1994) Cosmic ray contributions to dose rates for luminescence and ESR dating: large depths and long-term time variations. *Radiation Measurements*, 23, 497–500. Available from: https://doi.org/10.1016/1350-4487(94)90086-8

Richard, M., Falguères, C., Pons-Branchu, E., Ghaleb, B., Valladas, H. & Mercier, N. *et al*. (2017) Datation par les méthodes ESR/U-Th combinées de sites du Pléistocène supérieur: méthodologie et application en contexte karstique. *Anthropologie*, 121, 63–72. Available from: https://doi.org/10.1016/j.anthro.2017.03.006

Romagnoli, F., Chabai, V., Gravina, B., Hérisson, D., Hovers, E. & Moncel, M.H. *et al*. (2022) Neanderthal technological variability: a wide-ranging geographical perspective on the final Middle Palaeolithic. In: Romagnoli, F., Rivals, F. & Benazzi, S. (Eds.), *Updating*

Neanderthals: Understanding Behavioural Complexity in the Late Middle Palaeolithic. Cambridge: Academic Press. Available from: https://doi.org/10.1016/B978-0-12-821428-2.00012-3

Schreve, D.C., Bridgland, D.R., Allen, P., Blackford, J.J., Gleed-Owen, C.P., Griffiths, H.I. *et al.* (2002) Sedimentology, palaeontology and archaeology of late Middle Pleistocene River Thames terrace deposits at Purfleet, Essex, UK. *Quaternary Science Reviews*, 21, 1423–1464. Available from: https://doi.org/10.1016/S0277-3791(01)00100-7

Scott, B., Ashton, N., Penkman, K.E.H., Preece, R.C. & White, M. (2010) The position and context of Middle Palaeolithic industries from the Ebbsfleet Valley, Kent, UK. *Journal of Quaternary Science*, 25, 931–944.

Shao, Q., Bahain, J.-J., Falguères, C., Dolo, J.-M. & Garcia, T. (2012) A new U-uptake model for combined ESR/U-series dating of tooth enamel. *Quaternary Geochronology*, 10, 406–411. Available from: https://doi.org/10.1016/j.quageo.2012.02.009

Silvestrini, M., Bassetti, M., Boscato, P., Coltorti, M., Esu, D., Lemorini, C. *et al.* (2001) An Acheulean site of the last Interglacial at Boccabianca (Cupra Marittima, Marche Region, Italy). *Rivista di Scienze Preistoriche*, LI, 21–71.

Soriano, S. & Villa, P. (2017) Early Levallois and the beginning of the Middle Paleolithic in central Italy. *PLoS One*, 12(10), e0186082. Available from: https://doi.org/10.1371/journal.pone.0186082

Taschini, M. (1967) Il "Protopontiniano" rissiano di Sedia del Diavolo e di Monte delle Gioie (Roma). *Quaternaria*, 9, 301–319.

Van Baelen, A., Meijs, E.P.M., Van Peer, P., de Warrimont, J.P. & De Bie, M. (2008) The early Middle Palaeolithic site of Kesselt-Op de Schans (Belgian Limburg). Excavation campaign 2008. *Notae Praehistoricae*, 28, 5–9.

Villa, P., Soriano, S., Grün, R., Marra, F., Nomade, S., Pereira, A. *et al.* (2016) The Acheulian and Early Middle Paleolithic in Latium (Italy): stability and Innovation. *PLoS One*, 11(8), e0160516. Available from: https://doi.org/10.1371/journal.pone.0160516

Voinchet, P., Moreno, D., Bahain, J.J., Tissoux, H., Tombret, O., Falguères, C. *et al.* (2015) New chronological data (ESR and ESR/U-series) for the earliest Acheulian sites of north-western Europe. *Journal of Quaternary Science*, 30, 610–622. Available from: https://doi.org/10.1002/jqs.2814

Yokoyama, Y. & Nguyen, H. (1980) Direct and non-destructive dating of marine sediments, manganese nodules and corals by high resolution gamma-ray spectrometry. In: Goldberg, E.D. (Ed.) *Isotope Marine Chemistry*. Tokyo: Geochemistry Research Association, pp. 259–289.

Zorzi, F. & Pasa, A. (1945) Il deposito quaternario di Villa di Quinzano. *Bullettino di Paletnologia Italiana*, VIII, 1–52.